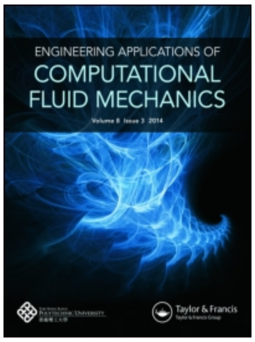

Engineering Applications of Computational Fluid Mechanics

ISSN: 1994-2060 (Print) 1997-003X (Online) Journal homepage: https://www.tandfonline.com/loi/tcfm20

Numerical simulation of nanofluid flow inside a root canal

Mohammad Ghalandari, Elaheh Mirzadeh Koohshahi, Fatemeh Mohamadian, Shahabbodin Shamshirband & Kwok Wing Chau

ENGINEERING APPLICATIONS OF COMPUTATIONAL FLUID MECHANICS
2019, VOL. 13, NO. 1, 254–264
https://doi.org/10.1080/19942060.2019.1578696

Taylor & Francis
Taylor & Francis Group

OPEN ACCESS Check for updates

Numerical simulation of nanofluid flow inside a root canal

Mohammad Ghalandari[a], Elaheh Mirzadeh Koohshahi[b], Fatemeh Mohamadian[c], Shahabbodin Shamshirband[d,e] and Kwok Wing Chau[f]

[a]Department of Aerospace Engineering, Sharif University of Technology, Tehran, Iran; [b]Department of Mechanical Engineering, Amirkabir University, Tehran, Iran; [c]School of Dentistry, Shahid Beheshti University of Medical Sciences, Tehran, Iran; [d]Department for Management of Science and Technology Development, Ton Duc Thang University, Ho Chi Minh City, Vietnam; [e]Faculty of Information Technology, Ton Duc Thang University, Ho Chi Minh City, Vietnam; [f]Department of Civil and Environmental Engineering, Hong Kong Polytechnic University, Hung Hom, Hong Kong

ABSTRACT

Silver nano particles have antimicrobial property which makes them appropriate for disinfection. Due to their antimicrobial feature, these particles are applicable for root canal irrigation. Fluid flow inside root canal and its appropriate circulation results in more efficient removal of microorganisms. Due to the very small dimensions of a root canal, performing experimental research is very difficult to identify the phenomena occurring in the root canal; therefore, numerical investigation will be very helpful to gain appropriate insight into the flow features of a root canal during irrigation for disinfection. Computation Fluid Dynamic (CFD) can be employed to numerically simulate the flow of irrigants inside the root canal. In the present study, the flow of Ag/water nanofluid in the root canal is numerically modeled. In order to evaluate the impact of height of injection and nanofluid concentration, two heights and concentrations are considered and compared. According to the results, lower injection height is more favorable due to better circulation of an irrigant in the root canal. Moreover, increase in the concentration of the nanofluid leads to reduction in maximum velocity of the fluid; which is attributed to higher increase in dynamic viscosity in comparison with the density. Velocity and wall shear stress contours in various cases are represented to gain better insight into the irrigant motion inside the canal. According to the results of simulation, wall shear stress of the root canal increases by increment in the concentration of the nanofluid and volumetric flow rate of the irrigants.

ARTICLE HISTORY
Received 16 December 2018
Accepted 1 February 2019

KEYWORDS
Computation fluid dynamic (CFD); root canal; nanofluid; dynamic viscosity

Nomenclature

g	Gravitational acceleration ($\boldsymbol{m/s^2}$)
V	Velocity
$\boldsymbol{S_m}$	Mass source or sink
$\boldsymbol{\mu}$	Dynamic viscosity
$\boldsymbol{\rho}$	Density

Subscript

nf	Nanofluid
f	Fluid
p	particle

1. Introduction

Disinfecting a root canal is an important stage in endodontic treatment. In order to have an appropriate removal of microorganisms, it is crucial to employ effective antimicrobial agents. Several irrigants have been tested in endodontic treatment to find their advantages and disadvantages (Akbarianrad, Mohammadian, Alhuyi Nazari, & Rahbani Nobar, 2018; Chan, Zhang, & Cheung, 2015). Silver nano particles have antimicrobial features and can be applied as an irrigant during endodontic treatment. As an example, Luna et al. (González-Luna et al., 2016) employed silver nano particles as final irrigant in endodontic. The case studies in their research were divided into four subgroups. Dispersed silver nano particles were used as the irrigant in the first group. In the second group, sodium hypochlorite (NaOCl) in 2.25% concentration was used as the irrigant. Combination of dispersed nano particles and ethylenediaminetetraacetic acid (EDTA) was applied in the third group, while saline water was used as the irrigant for the last group. According to the observations, both dispersed nano particles and NaOCl were appropriate for elimination of *Enterococcus faecalis*. Moghadas et al. (Moghadas, Narimani, & Shahmoradi, 2012) evaluated the performance of silver nano particles against *Staphylococcus aureus* and *E. fae-*

CONTACT Shahabbodin Shamshirband shahaboddin.shamshirband@tdtu.edu.vn

calis and compared it with 5.25% NaOCl as an irrigant. The results of the research revealed that the nano-based irrigant was as favorable as NaOCl in preventing the growth of bacteria in the root canal.

In addition to the type of irrigant, the irrigant flow inside the root canal affects the quality of disinfection. Better circulation of the irrigant is necessary to achieve more effective removal of microorganisms. According to the principles of fluid dynamics, the flow of an irrigant inside the root canal depends on several factors including the density, dynamic viscosity and mass flow rate. Computational Fluid Dynamic (CFD) is a powerful approach to obtain fluid flow and heat transfer in various geometries and systems (Alizadeh et al., 2018; Ramezanizadeh, Alhuyi Nazari, Ahmadi, & Chau, 2019). Up to now, most of the CFD-based studies have focused on its applications in engineering systems (Ezhilsabareesh, Rhee, & Samad, 2018; Villalpando, Reggio, & Ilinca, 2012); however, there are some studies which employed CFD in medical sciences (Borse, Bhushan, Walters, & Burgreen, 2018). For instance, Inthavong et al. (Inthavong, Wen, Tu, & Tian, 2009) employed CFD to investigate the influence of morphology of nasal cavities on heat transfer and flow of inhaled air (Inthavong et al., 2009).

In these cases experimental research are difficult, applying mathematical approaches, including analytical and numerical (Chau & Jiang, 2002; Ghahremannezhad & Vafai, 2018; Mou, He, Zhao, & Chau, 2017), is very helpful to overcome the related issues (Faizollahzadeh Ardabili et al., 2018; Wu & Chau, 2006). As mentioned earlier, CFD is applicable for modeling various fluid flows (Akbarian et al., 2018). As an example, Li (Li, 2009) applied CFD in order to analyze fluid flow in a 1-stage centrifugal fan. Comparison of experimental data and numerical results revealed the applicability of CFD in accurate flow modeling. Nakkina et al. (Rao Nakkina, Arul Prakash, & Saravana Kumar, 2016) used CFD for modeling the flow of fluid in spiral casing with various configurations. Zhang et al. (Zhang, Ma, Hong, Yang, & Fang, 2017) used CFD for modeling the flow of axial piston pump. The numerical results showed good agreement with the experimental data. Due to acceptable performance of CFD-based approaches in modeling fluid flows in different geometries, it can be useful to simulate irrigants flow inside a root canal.

The small size of a root canal and difficulties related to the experimental research, necessitate numerical investigation of fluid flow inside the root canal. Moreover, the impact of using antimicrobial nanofluid, as a novel irrigant, must be evaluated to obtain insight into its advantages and disadvantages. In this article, CFD is employed to model silver/water nanofluid as an irrigant in a root canal. The influences of injection height, concentration of the nanofluid and volumetric flow rate of the irrigant are investigated and discussed. More details on the modeling procedure and required assumptions such as boundary conditions are represented in the following sections.

2. Methodology

The first step in root canal irrigation modeling procedure is defining the geometry of both canal and the needle used for the irrigant injection. The dimensions and shape of the canal are considered similar to ref. (Kocharian, n.d.). The length of the canal is equal to 18 mm while the diameters at the apical pint and orifice are 0.45 and 1.57 mm, respectively. The internal and external diameters of the needle are assumed to be equal to 196 μm and 320 μm, respectively. The length of the needle is equal to 31 mm. The height of injection assumed in the present research is 3 mm from the bottom of the canal. The schematic of the model is shown in Figure 1.

The geometry of the domains are meshed to solve the equations. In the current study, structured mesh are used for the modeling. After evaluating the grid independency, the optimal number of mesh is selected. The meshed domain is shown in Figure 2. The total number of elements in optimal condition is equal to 276209.

In order to determine the velocity field and fluid flow inside the canal, both mass and momentum conservations are numerically solved. The mass conservation equation is represented in Eq. 1 (Alizadeh, Ghasempour, Razi Astaraei, & Alhuyi Nazari, 2016).

$$\frac{\partial \rho}{\partial t} + \nabla.(\rho \vec{v}) = S_m \tag{1}$$

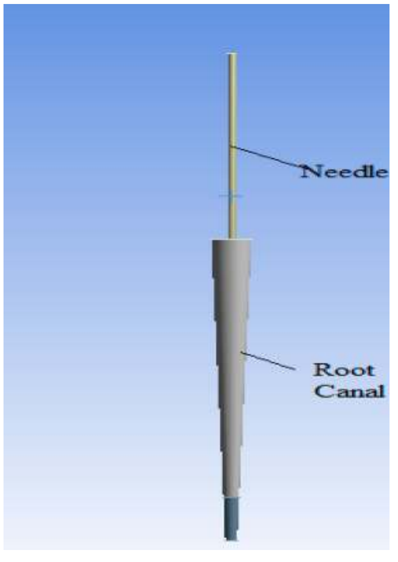

Figure 1. Schematic of the model.

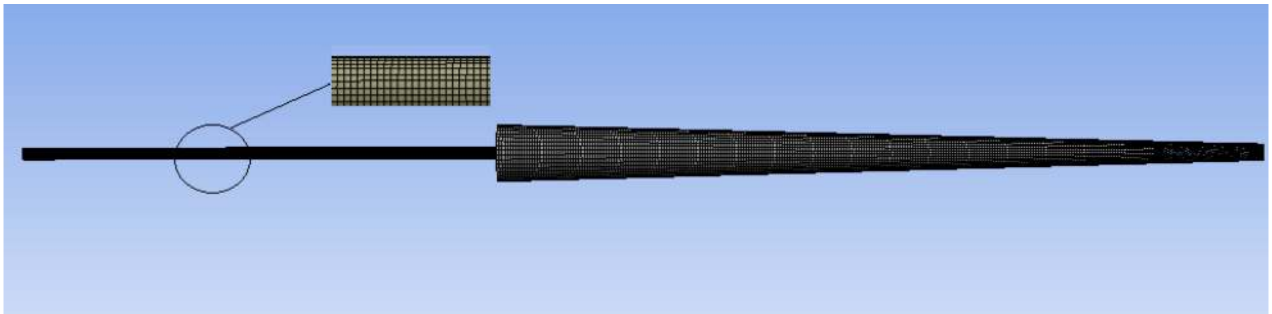

Figure 2. Domain with structured mesh.

Where S_m, ρ, and $\vec{v}$ stand for mass sink or source in the domain of flow, density of the irrigant and the vector of velocity, respectively. The utilized equation for momentum conservation is:

$$\frac{\partial(\rho\vec{v})}{\partial t} + \nabla.(\rho\vec{v}.\vec{v}) = -\nabla p + \nabla.\bar{\bar{\tau}} + \rho\vec{g} + \vec{F} \quad (2)$$

Where ρ, p, and $\rho\vec{g}$ are the fluid's density, pressure field and the body force due to gravitional acceleration, respectively. Moreover, $\vec{F}$ and $\bar{\bar{\tau}}$ refer to external force and the tensor of stress, respectively. The stress tensor can be obtained as:

$$\bar{\bar{\tau}} = \mu[(\nabla.\vec{v} + \nabla.\vec{v}^T) - \frac{2}{3}\nabla.\vec{v}.\bar{\bar{I}}] \quad (3)$$

Where μ and $\bar{\bar{I}}$ are dynamic viscosity and the unit tensor, respectively. The applied model for turbulence is k-ε. Details of this model is represented in Ref (Raisee, Noursadeghi, Hejazi, Khodaparast, & Besharati, 2007). It is assumed that the flow inside the root canal is incompressible and steady. The utilized boundary conditions for the wall of the canal is no slip. The inlet and outlet condition for the fluid flow in the needle are volumetric flow rate and pressure outlet. ANSYS CFX 17.0 is employed for solving the equations and numerical calculations. The defined criterion for convergence was residual lower than 10^{-5} for the applied equations.

Thermophysical features of nanofluids such as density and dynamic viscosity depend on the concentration and temperatures (M. H. Ahmadi et al., 2018; Mohammad Hossein Ahmadi, Ahmadi, Nazari, Mahian, & Ghasempour, 2018; Mohammad Hossein Ahmadi, Mirlohi, Alhuyi Nazari, & Ghasempour, 2018; Baghban, Jalali, Shafiee, Ahmadi, & Chau, 2019; Ramezanizadeh, Ahmadi, Ahmadi, & Alhuyi Nazari, 2018). In this study, it is assumed that the fluid flow is single phase, isothermal and the ambient temperature is 20°C. According to the literature review, the density of nanofluids can be determined as (Hemmat Esfe, Saedodin, Biglari, & Rostamian, 2016):

$$\rho_{nf} = \varphi\rho_p + (1-\varphi)\rho_f \quad (4)$$

In the above relationship, ρ_{nf}, ρ_p, and ρ_f are density of nanofluid, solid particles and the pure fluid, respectively. φ refers to the volumetric concentration of nano-sized solid particles in the base fluid. The data used for dynamic viscosity for the nanofluid are obtained from the study performed by Esfe et al. (Hemmat Esfe et al., 2016). In this study, the size of the particles is approximately 30-50 nm. The values of density for the base fluid and properties of the nano particles are shown in Table 1.

Table 1. Properties of the base fluid and nano particles (Hemmat Esfe et al., 2016).

Nano particle density (g/cm^3)	10.5
Water density (g/cm^3)	0.998
Shape of nano particles	Spherical
Color of particles	Black
Water viscosity (cP)	0.89

3. Results and Discussion

In this section, the results of the numerical simulation are represented and discussed. Two concentrations, including 0.01 and 0.0025 are considered in simulation and the obtained results are compared with pure water. Moreover, the influence of volumetric flow rate on the contour of velocity is investigated. First of all, the obtained results in the case of using water for irrigation is represented. As shown in Figure 1 Schematic of the model

Figure 3, when the volumetric flow rate is equal to 0.15 mL/s, the maximum velocity of the irrigant is equal to 5.865 m/s, while by increase in the flow rate to 0.25 mL/s, the highest velocity reaches 9.923 m/s. The highest velocity of irrigant exist in the needle; while its maximum value in the canal obtained at the outlet of the needle as it was anticipated. Since no slip boundary condition is assumed at the wall of the canal, increase in flow rate leads to higher velocity gradient which means improvement in wall shear stress.

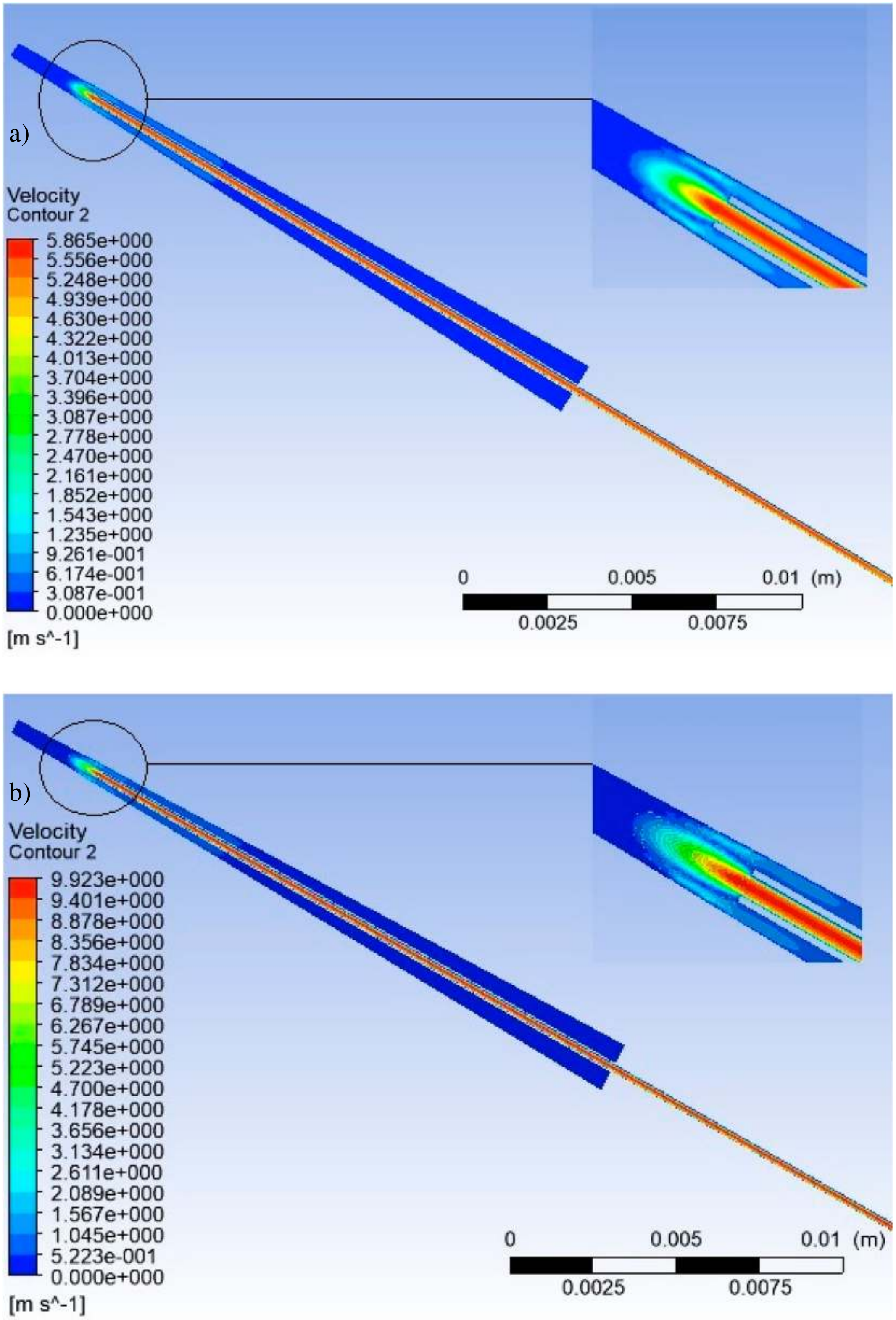

Figure 3. Velocity contours for water with volumetric flow rate of (a) 0.15 mL/s, (b) 0.25 mL/s

In addition to the velocity contours, the wall shear stress is another factor which influences on the quality of disinfection. Measurement of shear stress on the wall of the canal is very difficult due to its very small size and dimensions; therefore, CFD can be very useful for obtaining its values at different locations (Kocharian,

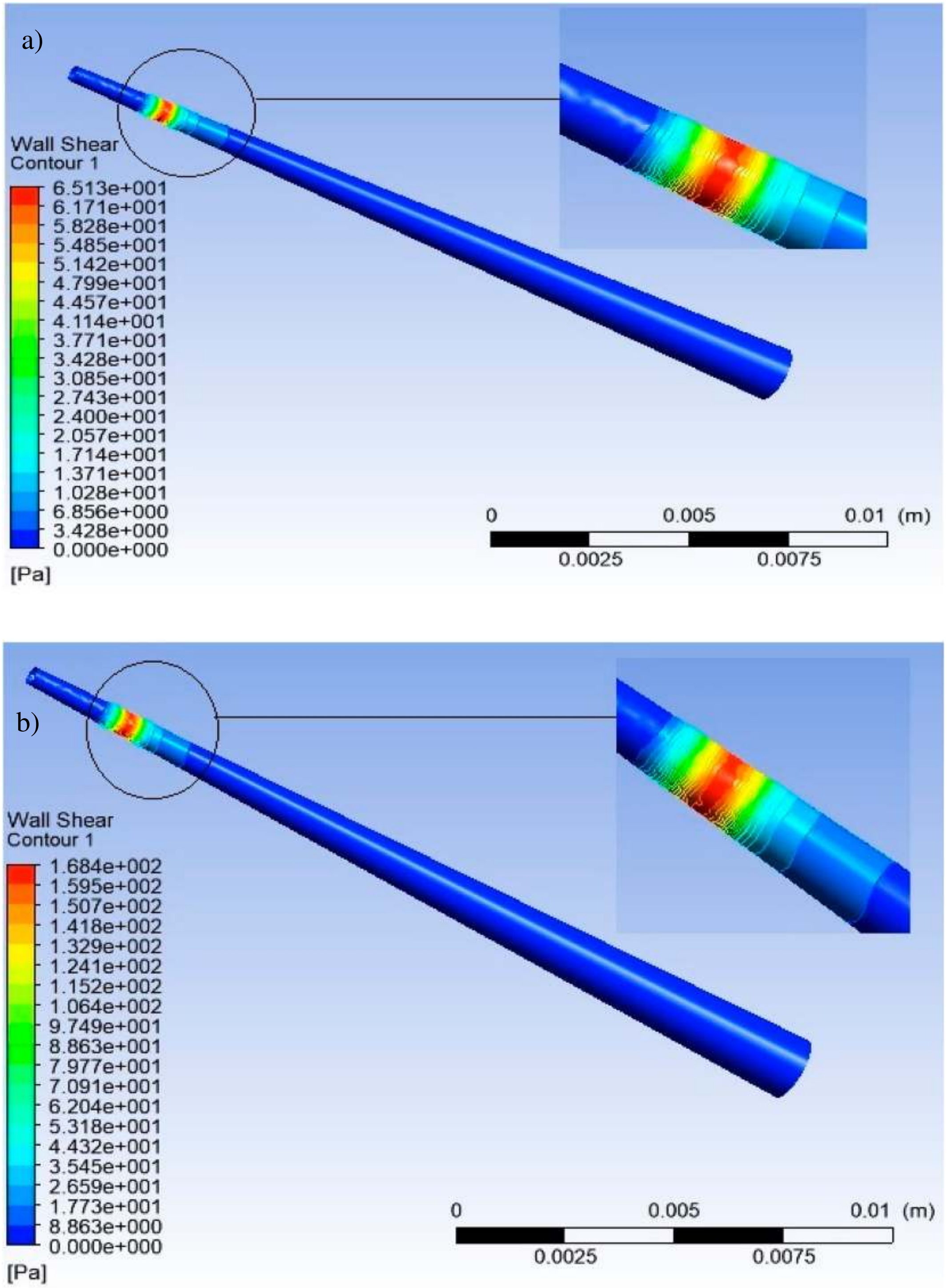

Figure 4. wall shear stress for water as irrigant in (a) 0.15 mL/s, and (b) 0.25 mL/s

n.d.). Shear stress at the wall of a root canal act as a force in tangential direction which has influence on debridement of the wall (Kocharian, n.d.). Lack of force in tangential direction means inappropriate debridement. Increase in the wall shear stress means better disinfection. In order to evaluate the impact of flow rate on the wall shear stress, the related contours are obtained for both cases as shown in Figure 4. As it is illustrated, increase in volumetric flow rate from 0.15 mL/s to 0.25 mL/s results in increment in maximum wall shear stress from approximately 65 Pa to 168 Pa. Since higher shear stress indicates improved disinfection, increase in flow rate is

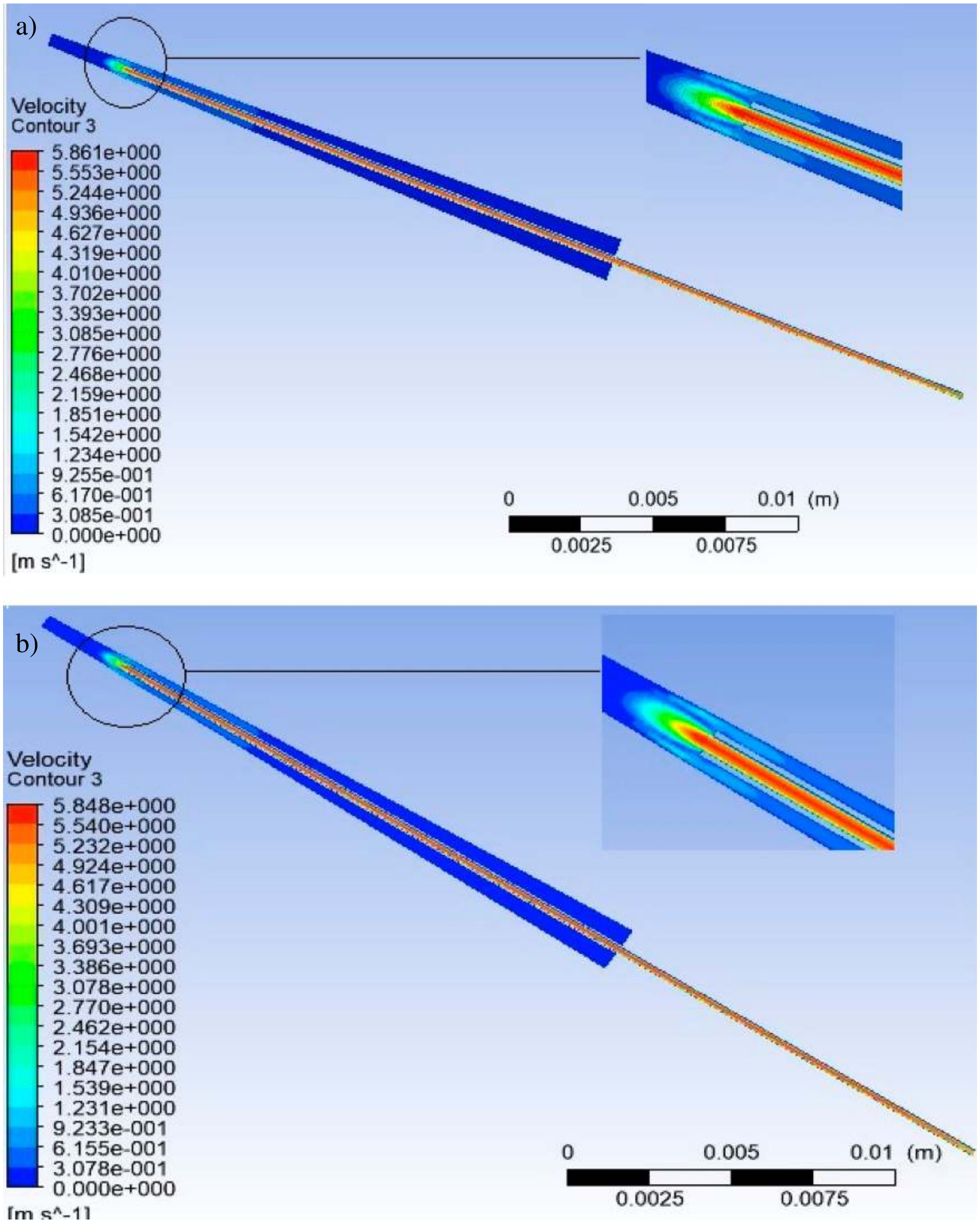

Figure 5. Velocity contours for nanofluid with volumetric flow rate of 0.15 mL/s and concentration of (a) 0.0025, (b) 0.01.

recommended to enhance the quality of microorganism removal.

In order to evaluate the influence of adding nano particles into the water on fluid flow, the velocity contours for the nanofluids in two concentrations, 0.0025 and 0.01, are obtained. In the case of 0.15 mL/s volumetric flow rate, as illustrated in Figure 5, the highest velocities of the nanofluids inside the canal are 5.861 and 5.848 m/s for 0.0025 and 0.01 volumetric concentrations, respectively. As shown in Figure 6, when the volumetric flow rate is 0.25 mL/s, the maximum velocities for the nanofluids with 0.0025 and 0.01 volumetric concentrations are 9.917 and 9.896 m/s, respectively. Higher velocity of the nanofluid with lower concentration can be attributed to its lower dynamic viscosity. Since the acting forces on the irrigant are gravitional and friction, and the increased ratio in the dynamic viscosity is higher than density, the maximum velocity of the nanofluid with 0.01

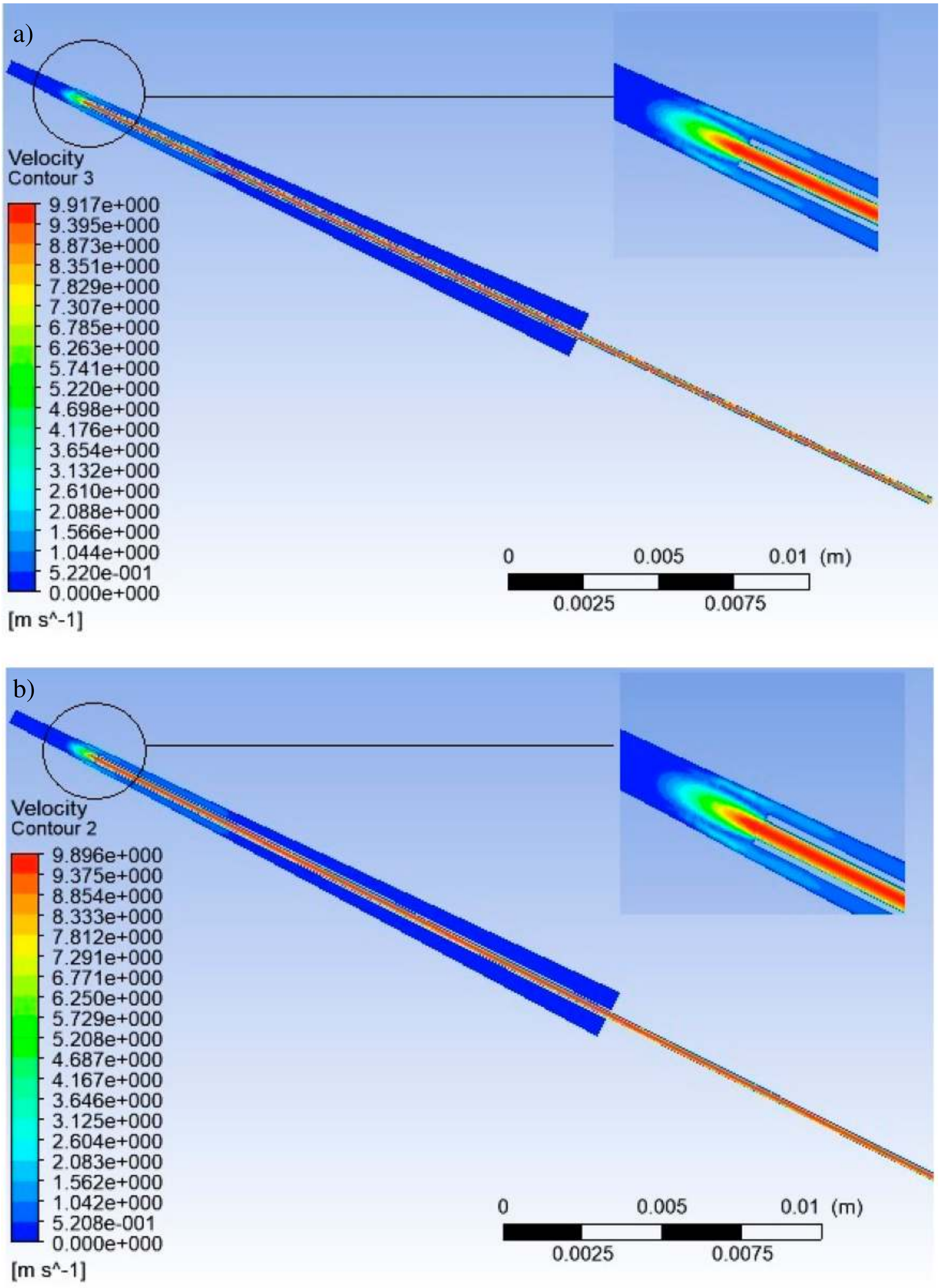

Figure 6. Velocity contours for nanofluid with volumetric flow rate of 0.25 mL/s and concentration of (a) 0.0025, (b) 0.01.

concentration is lower than the concentration of 0.0025 (since no slip boundary condition is assumed at the wall of the needle).

Similar to the case of using water, the wall shear stress contours are determined for the nanofluids as irrigants as shown in Figure 7 and Figure 8. In the cases of 0.15 mL/s

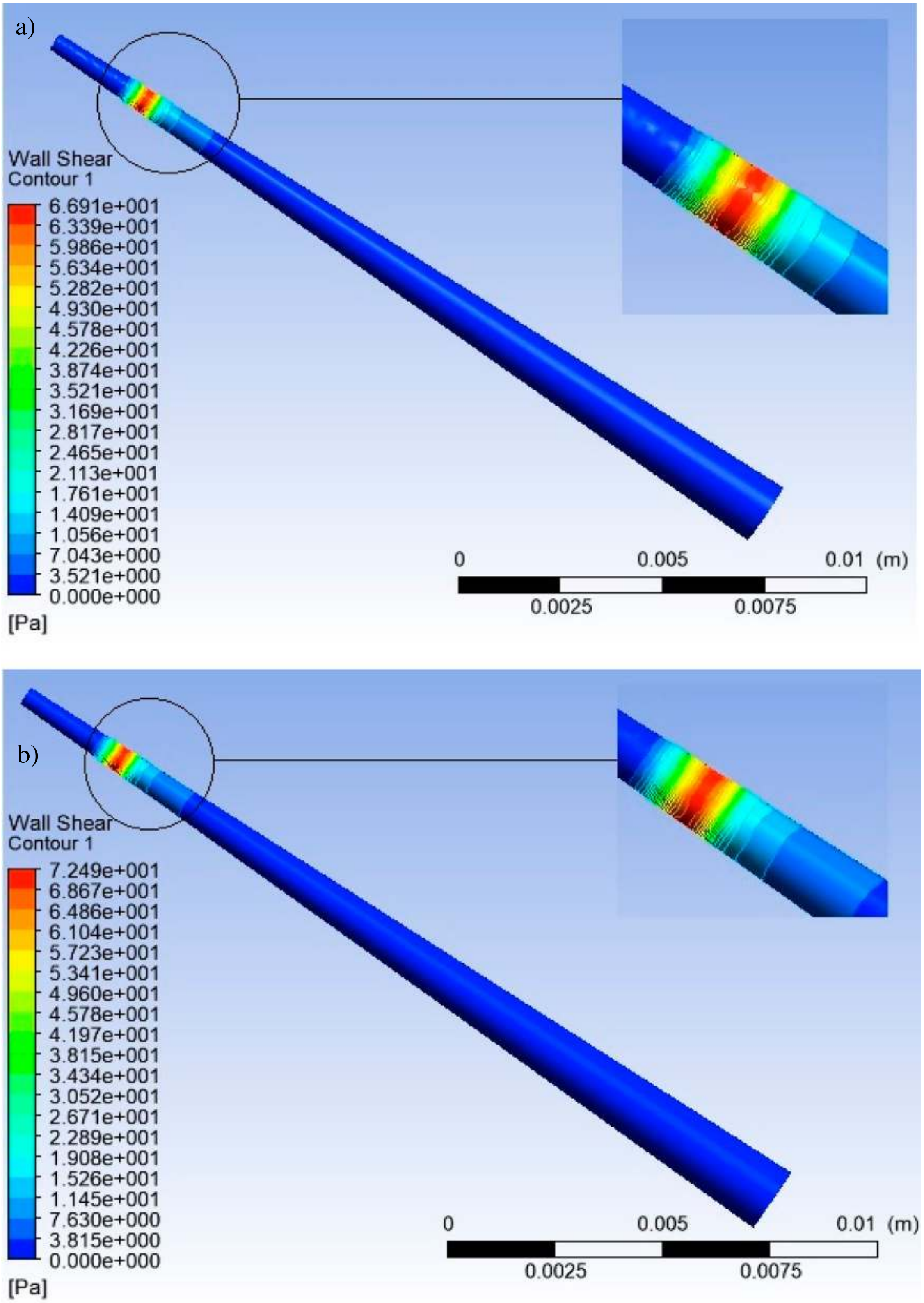

Figure 7. Wall shear stress contours for nanofluid with volumetric flow rate of 0.15 mL/s and concentration of (a) 0.0025, (b) 0.01.

volumetric flow rate of the nanofluid, the maximum wall shear stress for 0.0025 and 0.01 volumetric concentrations are 66.91 and 72.49 *Pa*, respectively. These values are higher than the corresponded value of water as irrigant which is 65.13 Pa. In Figure 8, the wall shear stress for the nanofluids is illustrated. The volumetric flow rate

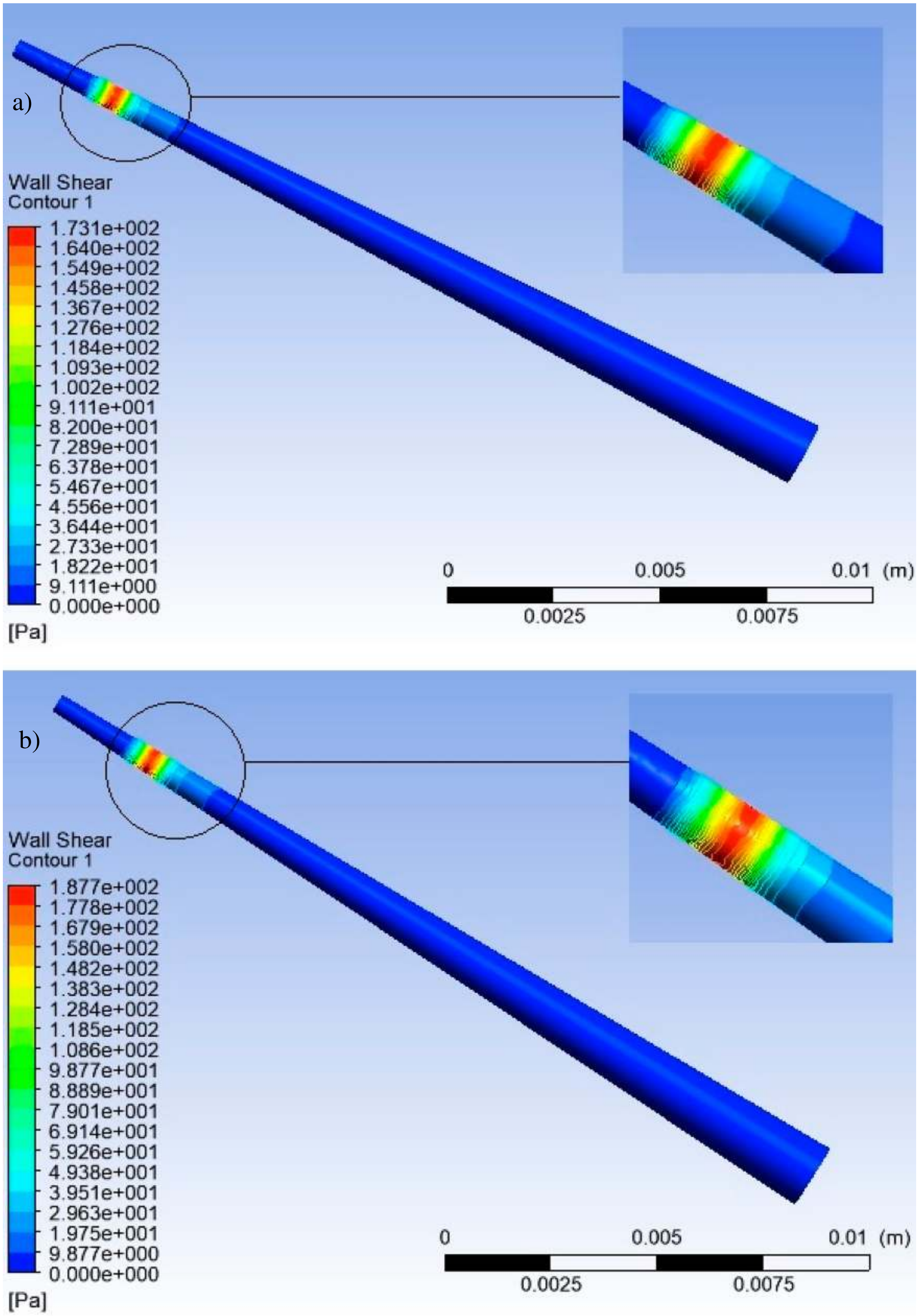

Figure 8. Wall shear stress contours for nanofluid with volumetric flow rate of 0.25 mL/s and concentration of (a) 0.0025, (b) 0.01.

in this case is equal to 0.25 mL/s. As shown in Figure 8, increase in dynamic viscosity results in improved wall shear stress in both concentrations in comparison with pure water as irrigant. Increased wall shear stress is attributed to enhanced dynamic viscosity. Therefore, it can be concluded that higher concentration of nanofluids can be more appropriate on the basis of increment in antimicrobial phase and wall shear stress.

4. Conclusion

In this article, fluid flow inside root canal was investigated. Applied irrigants were pure water, Ag/water nanofluid, which is an antimicrobial agent, in 0.01 and 0.0025 volume concentrations. Two volumetric flow rates including 0.15 and 0.25 mL/s were considered to assess its effect on velocity and wall shear stress. The results of numerical simulation indicated increase in concentration of the nanofluid led to reduction in velocity which was attributed to dynamic viscosity increase and no slip boundary condition. However, the wall shear stress increased by volumetric concentration mainly due to improved dynamic viscosity. According to the obtained data, increase in flow rate is recommended for root canal disinfection due to better circulation of irrigant inside the root canal and enhanced wall shear stress which means better removal of microorganisms. According to the simulation results, increment in the concentration of the nanofluids led to higher wall shear stress which is mainly due to increased dynamic viscosity of the nanofluid. Although the features of fluid flow inside the root canal are obtained successfully, experimental results are required to more accurately evaluate the utilized model. Future studies should focus on various shape and geometry of root canals and needles. Moreover, investigating the influence of injection height can be very useful to obtain insight into its impact in order to achieve more efficient disinfection.

Disclosure statement

No potential conflict of interest was reported by the authors.

References

Ahmadi, M. H., Ahmadi, M. A., Nazari, M. A., Mahian, O., & Ghasempour, R. (2018). A proposed model to predict thermal conductivity ratio of Al2O3/EG nanofluid by applying least squares support vector machine (LSSVM) and genetic algorithm as a connectionist approach. *Journal of Thermal Analysis and Calorimetry*, 1–11. doi:10.1007/s10973-018-7035-z

Ahmadi, M. H., Alhuyi Nazari, M., Ghasempour, R., Madah, H., Shafii, M. B., & Ahmadi, M. A. (2018). Thermal conductivity ratio prediction of Al2O3/water nanofluidby applying connectionist methods. *Colloids and Surfaces A: Physicochemical and Engineering Aspects*, *541*, 154–164. doi:10.1016/j.colsurfa.2018.01.030

Ahmadi, M. H., Mirlohi, A., Alhuyi Nazari, M., & Ghasempour, R. (2018). A review of thermal conductivity of various nanofluids. *Journal of Molecular Liquids*, *265*, 181–188. doi:10.1016/J.MOLLIQ.2018.05.124

Akbarian, E., Najafi, B., Jafari, M., Faizollahzadeh Ardabili, S., Shamshirband, S., & Chau, K. (2018). Experimental and computational fluid dynamics-based numerical simulation of using natural gas in a dual-fueled diesel engine. *Engineering Applications of Computational Fluid Mechanics*, *12*(1), 517–534. doi:10.1080/19942060.2018.1472670

Akbarianrad, N., Mohammadian, F., Alhuyi Nazari, M., & Rahbani Nobar, B. (2018). Applications of nanotechnology in endodontic: A review. *Nanomedicine Journal*, *5*(3), 121–126. doi:10.22038/NMJ.2018.005.0001

Alizadeh, H., Ghasempour, R., Razi Astaraei, F., & Alhuyi Nazari, M. (2016). Numerical modeling of PV Cooling by using Pulsating heat Pipe. In *The 3rd International Conference and Exhibition on Solar Energy ICESE-2016*. Tehran.

Alizadeh, H., Ghasempour, R., Shafii, M. B., Ahmadi, M. H., Yan, W.-M., & Nazari, M. A. (2018). Numerical simulation of PV cooling by using single turn pulsating heat pipe. *International Journal of Heat and Mass Transfer*, *127*, 203–208. doi:10.1016/J.IJHEATMASSTRANSFER.2018.06.108

Baghban, A., Jalali, A., Shafiee, M., Ahmadi, M. H., & Chau, K. (2019). Developing an ANFIS-based swarm concept model for estimating the relative viscosity of nanofluids. *Engineering Applications of Computational Fluid Mechanics*, *13*(1), 26–39. doi:10.1080/19942060.2018.1542345

Borse, M., Bhushan, S., Walters, D. K., & Burgreen, G. W. (2018). Numerical simulations of flow pattern and particle trajectories in feline aorta for hypertrophic cardiomyopathy heart conditions. *Engineering Applications of Computational Fluid Mechanics*, *12*(1), 57–73. doi:10.1080/19942060.2017.1339640

Chan, E. L., Zhang, C., & Cheung, G. S. (2015). Cytotoxicity of a novel nano-silver particle endodontic irrigant. *Clinical, Cosmetic and Investigational Dentistry*, *7*, 65–74. doi:10.2147/CCIDE.S68874

Chau, K. W., & Jiang, Y. W. (2002). Three-dimensional pollutant transport model for the Pearl River Estuary. *Water Research*, *36*(8), 2029–2039. doi:10.1016/S0043-1354(01)00400-6

Ezhilsabareesh, K., Rhee, S. H., & Samad, A. (2018). Shape optimization of a bidirectional impulse turbine via surrogate models. *Engineering Applications of Computational Fluid Mechanics*, *12*(1), 1–12. doi:10.1080/19942060.2017.1330709

Faizollahzadeh Ardabili, S., Najafi, B., Shamshirband, S., Minaei Bidgoli, B., Deo, R. C., & Chau, K. (2018). Computational intelligence approach for modeling hydrogen production: A review. *Engineering Applications of Computational Fluid Mechanics*, *12*(1), 438–458. doi:10.1080/19942060.2018.1452296

Ghahremannezhad, A., & Vafai, K. (2018). Thermal and hydraulic performance enhancement of microchannel heat sinks utilizing porous substrates. *International Journal of Heat and Mass Transfer*, *122*, 1313–1326. doi:10.1016/J.IJHEATMASSTRANSFER.2018.02.024

Ghahremannezhad, A., Xu, H., Alhuyi Nazari, M., Hossein Ahmadi, M., & Vafai, K. (2019). Effect of porous substrates on thermohydraulic performance enhancement of double layer microchannel heat sinks. *International Journal of Heat and Mass Transfer*, *131*, 52–63. doi:10.1016/J.IJHEATMASSTRANSFER.2018.11.040

González-Luna, P.-I., Martínez-Castañón, G.-A., Zavala-Alonso, N.-V., Patiño-Marin, N., Niño-Martínez, N., Morán-Martínez, J., & Ramírez-González, J.-H. (2016). Bactericide effect of silver Nanoparticles as a final irrigation agent in Endodontics on *Enterococcus faecalis*: An *Ex Vivo* study. *Journal of Nanomaterials*, *2016*, 1–7. doi:10.1155/2016/7597295

Hemmat Esfe, M., Saedodin, S., Biglari, M., & Rostamian, H. (2016). An experimental study on thermophysical properties and heat transfer characteristics of low volume concentrations of Ag-water nanofluid. *International Communications in Heat and Mass Transfer*, *74*, 91–97. doi:10.1016/J.ICHEATMASSTRANSFER.2016.03.004

Inthavong, K., Wen, J., Tu, J., & Tian, Z. (2009). From CT Scans to CFD Modelling – fluid and heat transfer in a Realistic Human nasal Cavity. *Engineering Applications of Computational Fluid Mechanics*, *3*(3), 321–335. doi:10.1080/19942060.2009.11015274

Kocharian, T. (n.d.). *Root canal irrigation- An engineering analysis using computational fluid dynamics*. Toronto: University of Toronto.

Li, H. (2009). Fluid flow Analysis of a single-stage centrifugal Fan with a Ported Diffuser. *Engineering Applications of Computational Fluid Mechanics*, *3*(2), 147–163. doi:10.1080/19942060.2009.11015261

Moghadas, L., Narimani, T., & Shahmoradi, M. (2012). Antimicrobial activity of a new nanobased endodontic irrigation solution: In vitro study. *Dental Hypotheses*, *3*(4), 142–146. doi:10.4103/2155-8213.106838

Mou, B., He, B.-J., Zhao, D.-X., & Chau, K. (2017). Numerical simulation of the effects of building dimensional variation on wind pressure distribution. *Engineering Applications of Computational Fluid Mechanics*, *11*(1), 293–309. doi:10.1080/19942060.2017.1281845

Mutlu, Y., & Çakan, M. (2018). Evaluation of in-pipe turbine performance for turbo solenoid valve system. *Engineering Applications of Computational Fluid Mechanics*, *12*(1), 625–634. doi:10.1080/19942060.2018.1506364

Raisee, M., Noursadeghi, a., Hejazi, B., Khodaparast, S., & Besharati, S. (2007). Simulation of Turbulent heat transfer In Jet Impingement of Air flow Onto A Flat wall. *Engineering Applications of Computational Fluid Mechanics*, *1*(4), 314–324. doi:10.1080/19942060.2007.11015202

Ramezanizadeh, M., Ahmadi, M. A., Ahmadi, M. H., & Alhuyi Nazari, M. (2018). Rigorous smart model for predicting dynamic viscosity of Al2O3/water nanofluid. *Journal of Thermal Analysis and Calorimetry*, *1*, 1–10. doi:10.1007/s10973-018-7916-1

Ramezanizadeh, M., Alhuyi Nazari, M., Ahmadi, M. H., & Chau, K. (2019). Experimental and numerical analysis of a nanofluidic thermosyphon heat exchanger. *Engineering Applications of Computational Fluid Mechanics*, *13*(1), 40–47. doi:10.1080/19942060.2018.1518272

Rao Nakkina, P., Arul Prakash, K., & Saravana Kumar, G. (2016). Numerical studies on fluid flow characteristics through different configurations of spiral casing. *Engineering Applications of Computational Fluid Mechanics*, *10*(1), 297–311. doi:10.1080/19942060.2016.1149103

Villalpando, F., Reggio, M., & Ilinca, A. (2012). Numerical study of flow around iced wind turbine airfoil. *Engineering Applications of Computational Fluid Mechanics*, *6*(1), 39–45. doi:10.1080/19942060.2012.11015401

Wu, C. L., & Chau, K. W. (2006). Mathematical model of water quality rehabilitation with rainwater utilisation: A case study at Haigang. *International Journal of Environment and Pollution*, *28*(3/4), 534–545. doi:10.1504/IJEP.2006.011227

Zhang, B., Ma, J., Hong, H., Yang, H., & Fang, Y. (2017). Analysis of the flow dynamics characteristics of an axial piston pump based on the computational fluid dynamics method. *Engineering Applications of Computational Fluid Mechanics*, *11*(1), 86–95. doi:10.80/19942060.2015.1091686